Journal of Applied Polymer Science

Preparation and properties of polycarbonate nanocomposites using attapulgite grafted poly(methyl methacrylate) as a potential nanofiller

Hang Xu,[1] Haicun Yang,[2] Liu Zhang,[1] Qingting Ni,[1] Fanghong Gong[1,3]

[1]College of Materials Science and Engineering, Changzhou University, Changzhou 213164, China
[2]Institute of Functional Polymers, School of Materials Science and Engineering, Tongji University, Shanghai 201804, China
[3]School of Mechanical Technology, Wuxi Institute of Technology, Wuxi 214121, China
Correspondence to: F. Gong (E-mail: fhgong@cczu.edu.cn)

ABSTRACT: The Core-shell hybrid particles with attapulgite (ATP) as the core and polymethylmethacrylate (PMMA) as the shell (ATP-*g*-PMMA) were prepared *via* reversible addition-fragmentation chain transfer (RAFT) polymerization method. The diameter of ATP-*g*-PMMA was increased to 50–60 nm, and the surface hygroscopicity was decreased observably after surface grafting. Then, ATP-*g*-PMMA hybrid particles were filled into the polycarbonate (PC) by melt mixing to afford nanocomposites, and the mechanical properties, microstructures, thermal stability, and rheological behavior of nanocomposites were investigated by varying ATP-*g*-PMMA concentration in the range 1, 3, 5, and 7 wt % in PC. Fourier Transform infrared spectroscopy (FTIR) suggested that there is no esterification reaction between particles and matrix. Slight changes in tensile strength, and noticeable decrease of elongation and impact strength were observed with the increase in ATP-*g*-PMMA particles loading. The morphology evaluated by field-emission scanning electron microscopy (FESEM) indicated that ATP-*g*-PMMA was dispersed with a diameter range of 80–100 nm, and phase separation was appeared with increasing ATP-*g*-PMMA loadings. Thermogravimetric analysis (TGA) results revealed the thermal stability of composites was strengthened. The disentanglement and interface slip induced by preferred orientation and directional arrangement of ATP-*g*-PMMA resulted in lower complex viscosity (η^*) and higher loss factor (tan δ) compared with the pristine PC.
 J. Appl. Polym. Sci. **2015**, *132*, 42262.

KEYWORDS: clay; composites; polycarbonates

Received 26 December 2014; accepted 22 March 2015
DOI: 10.1002/app.42262

INTRODUCTION

Over the past decades, polymer–clay nanocomposites have received big efforts because of their predicable improved properties and unexpected hybrid properties when compared with those of the pristine polymer or conventional composites.[1–3] According to previous researches, 3–5 wt % loading of nanoclay improves the mechanical and thermal properties of the polymer matrix to the same content as 30–50 wt % of other fillers under a homogeneous dispersion.[4,5] However, to achieve a homogeneous dispersion, proper surface modification of nano-clay is essential, and followed by melt blending or *in situ* polymerization process to improve the interfacial interaction between clay and polymer matrix.

Among the thermoplastic group of polymers, polycarbonate has been used in laboratories and industries due to its outstanding impact strength, optical transmittance, and formability.[6,7] However, the drawbacks of PC such as poor chemical resistance and high melt viscosity restrain its processing costs and operational life span.[8] So, modification in properties of PC to satisfy a specific requirement is an important proposition. At present, many different methods have been employed to modify PC for use in demanding applications, for example, bending with other polymers and changing the structure of macromolecules.[9–11]

As the development of nanocomposites technology, inorganic nanoparticles have also been applied in the modification of PC, particularly by using nanoclay mineral as a potential filler. The variations of thermal stability, mechanical properties, light transmission as well as crystallization behavior of nanocomposites in presence of nanoclay have been studied by many researchers. Wu *et al.*[12] prepared intercalated PC/clay nanocomposites by melt blending using epoxy resin as a compatibilizer. The addition of epoxy improved the dispersion of clay and enhanced the low-frequency viscoelastic response of nanocomposites. Wang *et al.*[13] reported the preparation of PC/acrylonitrile-butadiene-styrene (ABS) polymer alloy/montmorillonite (MMT) nanocomposites. An enhancement in thermal stability of the polymer matrix was noted in terms of the physical

barrier effect of intercalated MMT. Suin *et al.*[14–16] prepared exfoliated and optically transparent PC nanocomposites using phosphonium modified organoclay as potential nanofiller. The mechanical properties and thermal stability of nanocomposites were superior to that of neat PC. Moreover, the transparency was retained without development of any color. Rama *et al.*[17] prepared PC/MMT nanocomposites *via in situ* melt polycondensation, in which, MMT was modified by phosphonium and imidazolium based cations to functionalize without and with reactive functionality (bisphenol-A). The MMT containing reactive bisphenol-A groups resulted in the formation of exfoliated structure in contrast with the intercalated or phase separated structure of that without reactive functional groups. De la orden *et al.*[18] investigated the degradation of polymer during melt processing of clay reinforced PC nanocomposites. Effects of the chemical nature and the degree of dispersion of different clay into the polymer on the degradation of PC were more obvious than the other factors.

Attapulgite (ATP), also known as palygorskite, is a kind of hydrated aluminum–magnesium silicate mineral with a fibrous morphology and structural formula of $Si_8O_{20}Mg_5(Al)(OH)_2\ (H_2O)_4{\cdot}4H_2O$ which was first putted forward by Bradley.[19] To date, ATP has been widely used in agriculture, clay mineralogy, environmental protection, and catalyst engineering due to its excellent physical and chemical properties, together with a larger surface area and high aspect ratios.[20–23] Meanwhile, ATP has attracted much attention as polymer enforcement, polymer materials such as epoxy resins, polyaniline, polyamide-6, and polypropylene have been widely used as matrices in the design of polymer/ATP nanocomposites.[24–27] However, as reasonable nanofiller with few reports devoted to the nanocomposites of PC. Gao *et al.*[28] prepared ternary ATP/PP/PC nanocomposites with core-shell morphology *via* two-step melt blending process. The interfacial voiding and reinforcement of ATP were the main toughening effect in the ternary nanocomposites.

Summarizing the amount of researches on PC/clay nanocomposites above, in most cases, the morphology or the dispersion of clay, and the increase in melt viscosity of nanocomposites limited the application of PC/clay nanocomposites.[29,30] On the other hand, the thermal degradation during melt blending caused by water may be significantly aggravated in presence of hydrophilic clay.[31,32] Therefore, the organic modification of clay, and the introduction of the third portion such as ABS, epoxy and PMMA are most important in the preparation of PC/clay nanocomposites. For the surface grafting modification of ATP and the application in polymer, we have reported the preparation of ATP/polymer hybrids.[33,34] To obtain a prefer modification effect, in the present work, PMMA grafting ATP hybrids (ATP-*g*-PMMA) were prepared *via* RAFT graft polymerization technique, and then a series of polymer-clay nanocomposites consisting of PC and ATP-*g*-PMMA were prepared *via* melt blending method. The dispersion, mechanical properties, interaction between PC and ATP-*g*-PMMA, thermal and rheological properties were investigated in detail.

EXPERIMENTAL

Materials

Attapulgite (ATP) was obtained from Jiuchuan nano-material science (Jiangsu, China). It was dissociated with sodium hexametaphosphate solution of 3 wt %, activated with hydrochloric acid of 1 mol/L and then dried in a vacuum at 120°C for 36 h before use. Methyl methacrylate (MMA) and 2,2′-azobis(2-methylpropionitrile) (AIBN) were of synthetic grade and procured from Shanghai Chemical factory, China. MMA was passed through a column of basic alumina to remove inhibitors, and then distilled under reduced pressure. AIBN was purified by recrystallization from ethanol and stored at −15°C. γ-methacryloxypropyl trimethoxysilane (MPS, 98%) was used as received from Aladdin reagent (Shanghai, China). Cyanopropyl dithiobenzoate (CPDB) was synthesized according to the literature reported previously.[35] Polycarbonate (PC, S-2001R) used in this study was of commercial grade purchased from Mitsubishi Engineering-Plastics Corp. The viscosity-average molecular weight was 2.3×10^4 g/mol, and melt flow rate (MFR) was 7.5–10.5 g/10 min at 300°C and 1.2 kg load. All solvent were analytical grade and used as received from Sinopharm Chemical Reagent (Shanghai, China).

Synthesis of ATP-*g*-PMMA Hybrid Particles *via* RAFT Polymerization

The methacryl functionalized attapulgite (ATP-MPS) was prepared by a silanization. A typical procedure was as follows, in a 250 mL round bottom flask, 2 g of activated ATP was suspended in 150 mL of xylene under stirring and ultrasonic vibration for 60 min to obtain a homogeneous dispersion. The mixture obtained was heated to boil for 20 min and then cooled to 70°C, 4 mL of MPS was added to the flask. Surface treatment was carried out for 10 h under nitrogen atmosphere with a strong mechanical stirring. After reaction, the mixture was filtered and the sediment was washed several times with ethanol to remove unreacted MPS. The resulting ATP-MPS was dried in a vacuum oven at 40°C. Grafting of ATP-MPS with PMMA (ATP-*g*-PMMA) was achieved by RAFT technique. 1.5 g of ATP-MPS was mixed with 20 mL of *N*,*N*-dimethylformamide (DMF) *via* ultrasonic dispersion method in a 100 mL single-neck round-bottom flask, and then 14.8 mL of MMA, 64.8 μL of CPDB, and 28.7 mg of AIBN were added. After deoxygenating by purging with continuous nitrogen gas, the flask was sealed and heated at 70°C for 8 h in an oil bath. After reaction, the mixture was diluted with DMF and centrifugated, the solid products were washed with tetrahydrofuran (THF) for several times to remove homopolymer. Finally, the resulting ATP-*g*-PMMA was dried in a vacuum oven at 50°C. The molecular weight and polydispersity index (PDI) of grafting PMMA were 35,800 g/mol and 1.22, respectively, calculated from gel permeation chromatography (GPC) analysis.

Preparation of ATP-*g*-PMMA Hybrids

After completely drying in a vacuum oven at 90°C over 24 h, PC was melt blended with ATP-*g*-PMMA hybrid particles and a small amount of antioxidant using a Haake minilab twin-screw micro extruder at 260°C. The obtained nanocomposites were first heated at 260°C for 3 min under a rapid compression, followed by release of pressure to remove any gas bubbles (XLB-D350×350×2, Changzhou, China). The composites were then modeled under 6–7 ton pressure for 4 min and cooled between two water chilled aluminum plates. Specimens with different

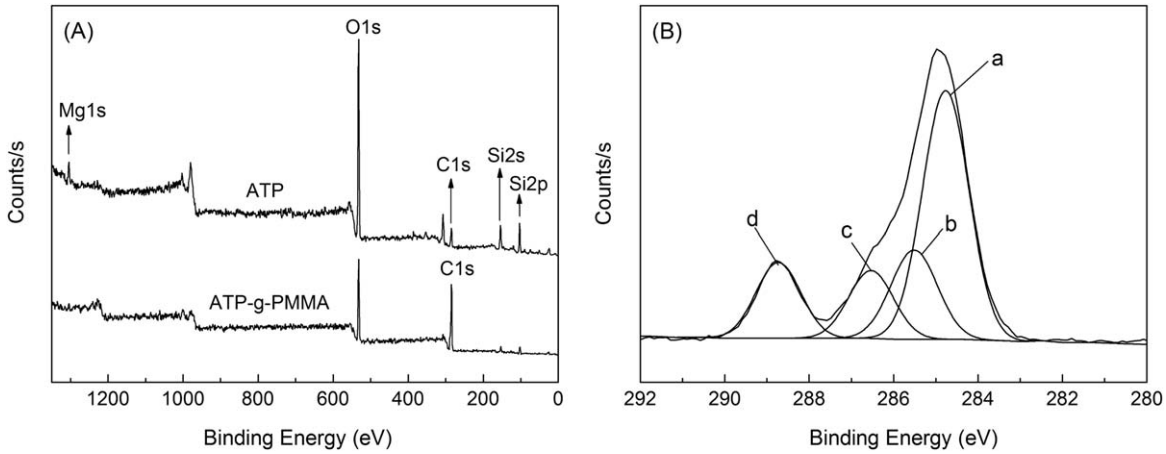

Figure 1. (A) XPS full-scan spectrum of ATP and ATP-*g*-PMMA, (B) C1s core-level spectra of ATP-*g*-PMMA.

dimensions in thickness were cut from plaques for the different measurements.

Characterization

Changes in the surface chemical composition of ATP, ATP-MPS, and ATP-*g*-PMMA were analyzed by using an Escalab 250Xi X-ray Photoelectron spectrometer (XPS, Thermo Fisher) in an ultra high vacuum with Al Kα radiation. Wide angle X-ray diffraction was carried out on a D/max-2500PC rotating anode X-ray generator (XRD, Rigaku, Japan) with Cu Kα radiation operated at 40 kV and 100 mA. Transmission electron microscopy was carried out by a JEM-1200 EX/S transmission electron microscope (TEM, JEOL, Japan) with an accelerating voltage of 200 kV. Thermogravimetric analysis was carried out using a TG209 F3 system (TGA, Netzsch, Germany) within the temperature range of 50–800°C at a heating-up rate of 10°C/min under a continuous nitrogen flow. Fourier transform infrared spectra were collected by an Avatar 370 FTIR spectrometer (FTIR, Nicolet). Tensile test was carried out at room temperature on a WDT-10 universal material tester (Shenzhen, China). Tensile properties were performed according to the GB/T 1040–1992 standard method. Impact strength was measured according to the GB/T 1845–1993 standard method on an XJU-22 Izod impact tester (Chengde, China). MFR was measured at 300°C under 1.26 kg using a MTM1000-A1 melt-flow indexer (Shenzhen, China). The morphology of fracture surface was studied using a SUPRA55 field emission scanning electronic microscope (FESEM, Zeiss, Germany). All the specimens were coated with gold before viewing. Rheological measurements were performed on a MCR301 rotational rheometer (Anton Paar, Germany) at 260°C, using parallel plate geometry (50 mm diameter) with a gap between the two plates of 1 mm.

RESULTS AND DISCUSSION

Preparation and Characterization of ATP-*g*-PMMA Hybrids

XPS was used to characterize the PMMA layer on the surface of ATP. Figure 1 shows the XPS full-scan spectrum of ATP and ATP-*g*-PMMA. The wide-scan spectrum of ATP is dominated by silicon (103.3 eV, Si2p; 154.4 eV, Si2s), magnesium (1304.4 eV, Mg1s), carbon (284.9 ev, C1s), and oxygen (531.8 eV, O1s) elements. After surface grafting, the C element increases obviously in the spectrum of ATP-*g*-PMMA, which results from the high carbon content of PMMA [Figure 1(A)]. In the narrow scan of C1s core-level spectra of ATP-*g*-PMMA [Figure 1(B)], the C1s peak resolves four peaks representing different carbons environment in PMMA: (a) aliphatic hydrocarbon (C—C/CH) at a binding energy (BE) of 284.7 eV, (b) a *β*-shifted carbon combining with ester groups (C—COO) at 285.5 eV, (c) C—O of ester at 286.5 eV, and (d) the carboxyl carbon (C═O) at 288.7 eV.[36] On the basis of the above results, it could be concluded that ATP-*g*-PMMA hybrid particles were prepared successfully.

The XRD patterns in the 2θ range 5–40° are presented in Figure 2. It was observed that ATP has the main components phase with appreciable amounts of smectite, quartz and calcite. The reflections at $2\theta = 8.43°$ (110), 13.68° (200), and 16.28° (130) were associated with the characteristic *d* spacing of ATP. After surface grafting of PMMA, all of above reflections has almost no changes of position except for weak changes in peak intensity. It can be concluded that the crystal structure of ATP was maintained during RAFT graft polymerization process and the grafting PMMA was only anchored on the surface, and no PMMA was intercalated into the nano-channels of ATP.

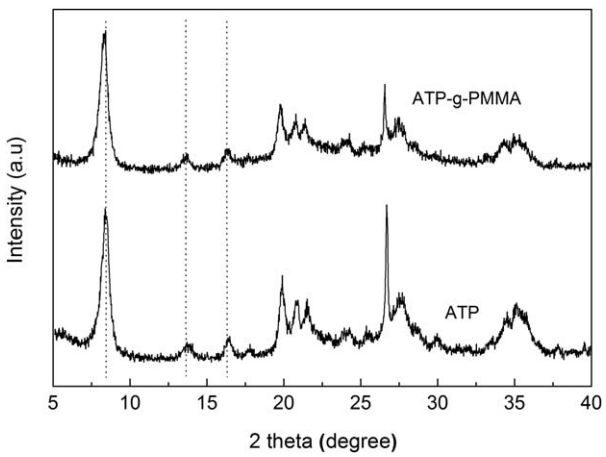

Figure 2. XRD patterns of ATP and ATP-*g*-PMMA.

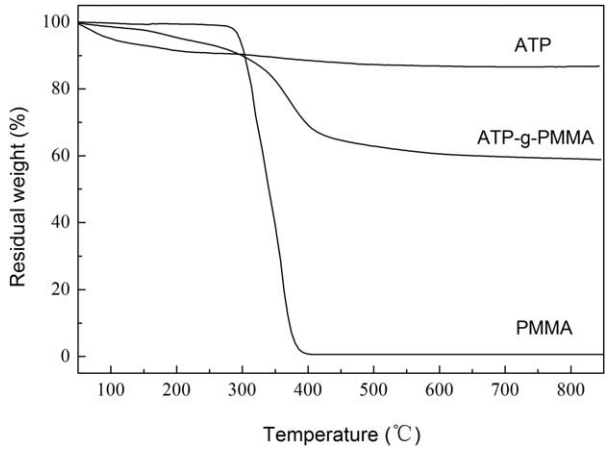

Figure 3. TGA curves of ATP, ATP-*g*-PMMA, and PMMA.

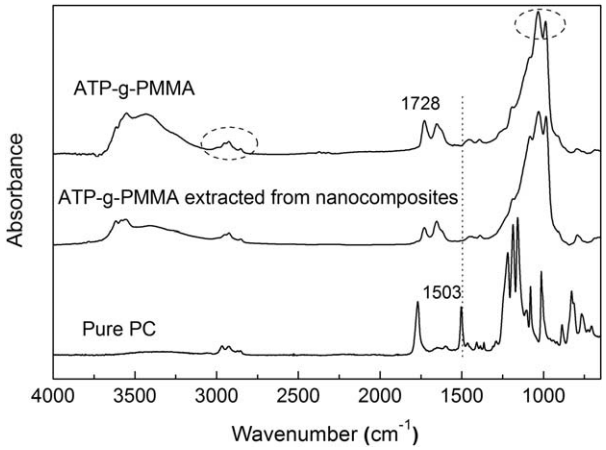

Figure 5. FTIR spectra of ATP-*g*-PMMA, PC, and ATP-*g*-PMMA extracted from nanocomposites.

The TGA results of ATP and ATP-*g*-PMMA are shown in Figure 3. It is observed that ATP loses 13.2% in the range of temperature from 50 to 850°C, which results from the release of absorbed water, zeolite water, crystal water, and structured water. After surface grafting of PMMA, it should be noticed that the weight loss of ATP-*g*-PMMA at the temperature before 200°C is decreased obviously compared with bare ATP. It confirmed that the hydrophilic surface of ATP is alleviated and consequently absorbed less moisture in presence of PMMA grafting layer, which may avoid the thermal degradation of polymer chains during the direct blending process of PC and hydrophilic clay. Despite the distinct characteristics between commercial PMMA and grafted PMMA such as Mw and molecular weight distribution, its degradation curve under same condition is plotted for comparison purpose. It is obvious that the degradation profile of ATP-*g*-PMMA is rather different from that of commercial PMMA. The weight loss around 200°C of ATP-*g*-PMMA is attributed to the thermal decomposition of oxyen-containing groups resulting from previous surface treatment of ATP. Further differences are also observed at higher temperature. The thermal degradation of commercial PMMA begins at 288°C and terminates at 400°C, whereas the grafted PMMA on the surface of particles is stable up to 330°C. The increase in thermal stability observed for the grafted PMMA may be ascribed to the ability of the ATP surface to annihilate free radicals generated during thermal decomposition.[37]

Figure 4 shows the TEM pictures of ATP and ATP-*g*-PMMA. According to Figure 4(A), it can be found that the nanofibers of bare ATP clay have relatively smooth surface with an average diameter of about 20 nm. It can be seen from Figure 4(B) that the diameter of ATP-*g*-PMMA is increased to around 50–60 nm, and a remarkable rough surface morphology can be observed after surface grafting of PMMA.

FTIR Analysis

Generally speaking, a number of grafting chains would be formed through the interchange esterification reaction of ester groups in PC and hydroxyl groups on the surface of nanoclay at high temperature. So, to investigate the interaction between PC and ATP-*g*-PMMA particles, chloroform was used as the eluant to extract ATP-*g*-PMMA particles form nanocomposites and the FTIR results are shown in Figure 5. The two sharp peaks at 982 cm^{-1} and 1029 cm^{-1} are assigned to Si—O stretching vibrations. The absorption peak at 1728 cm^{-1} is attributed to C═O stretching vibrations, and peaks in the range of 2800–3000 cm^{-1} correspond to the characteristic stretching of PMMA carbon chains. For pure PC, the peak at 1503 cm^{-1} represents the skeletal vibration of aromatic rings. However, the spectrum of ATP-*g*-PMMA extracted from nanocomposites does not present the characteristic peaks of aromatic rings, and it is nearly the same as ATP-*g*-PMMA particles. It can be concluded

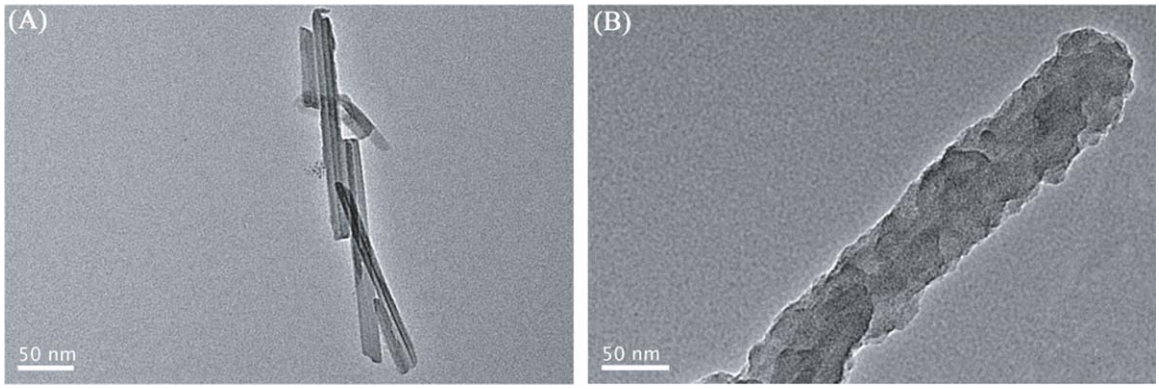

Figure 4. TEM images of (A) ATP and (B) ATP-*g*-PMMA. [Color figure can be viewed in the online issue, which is available at wileyonlinelibrary.com.]

Table I. Mechanical Properties of PC/ATP-*g*-PMMA Nanocomposites

Samples	Tensile strength (N/mm^2)	Elongation at break (%)	Impact strength (kJ/m^2)
PC	56.6	20.8	6.1
1 wt % ATP-*g*-PMMA	58.2	12.6	5.7
3 wt % ATP-*g*-PMMA	59.3	9.9	4.8
5 wt % ATP-*g*-PMMA	55.4	6.4	4.2
7 wt % ATP-*g*-PMMA	54.9	4.6	3.8

that there is no esterification reaction during melt blending, and thus the thermal degradation of PC matrix is avoided.

Mechanical Properties

The PC/ATP-*g*-PMMA nanocomposites were further evaluated by tensile and impact testing. Data pertaining to the tensile and impact properties are summarized in Table I. The changes in tensile strength of nanocomposites are not significant compared with that of PC, which may ascribe to the weaker interaction in nanocomposites. However, the elongation and impact strength decrease monotonically with increasing ATP-*g*-PMMA loading. ATP is a kind of natural fibrous rod-like nanoparticle with high rigidity, PMMA is a typical fragile material, and therefore plastic deformation for ATP-*g*-PMMA particles is more difficult. This means that the absorbed energy of PC continuous phase is decreased, resulting in an easier fracture under applied stress. In other words, the brittleness of nanocomposites is enhanced.

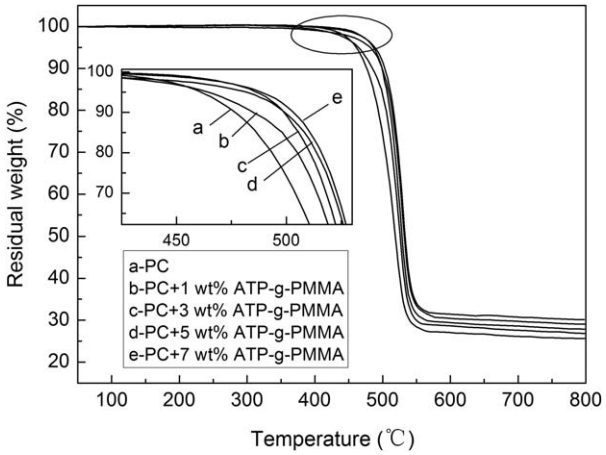

Figure 6. TGA curves of pristine PC and nanocomposites with different contents of ATP-*g*-PMMA.

Thermal Properties

The thermal stability of pristine PC and nanocomposites with different particle loadings was investigated by thermogravimetric

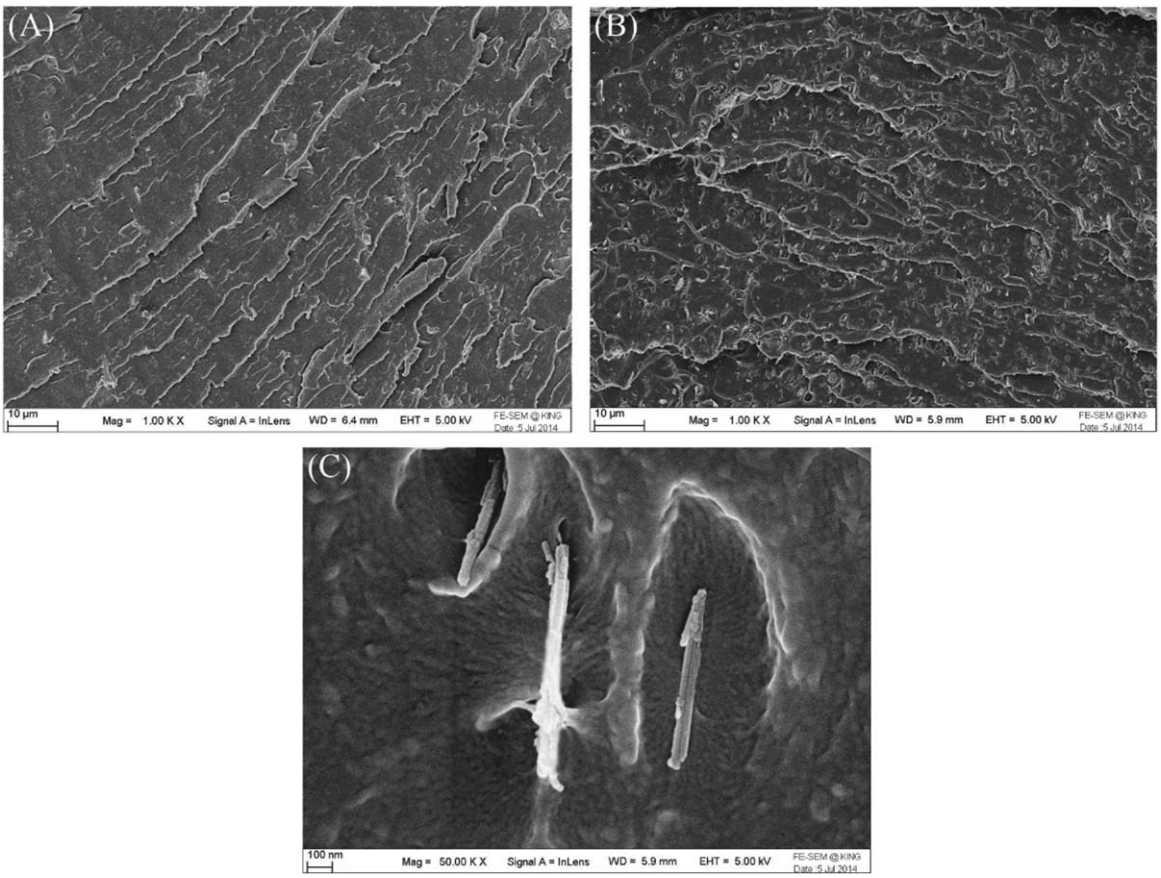

Figure 7. FESEM images of fracture surface of (A) 1 wt % PC/ATP-*g*-PMMA, (B and C) 5 wt % PC/ATP-*g*-PMMA nanocomposites. [Color figure can be viewed in the online issue, which is available at wileyonlinelibrary.com.]

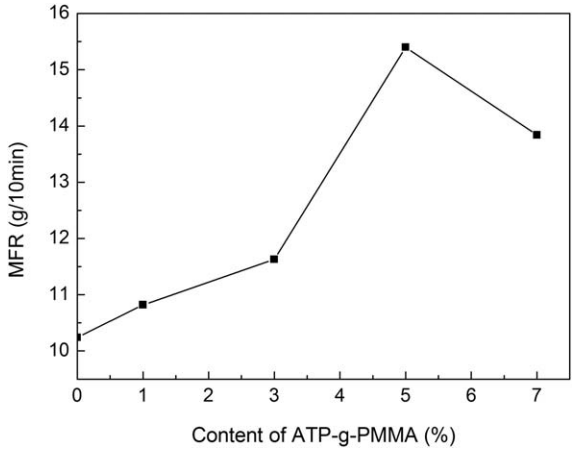

Figure 8. MFR of PC and nanocomposites with different contents of ATP-*g*-PMMA.

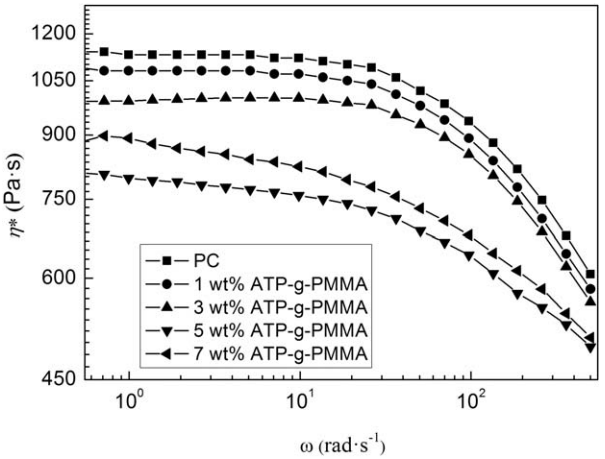

Figure 9. Dependence of complex viscosity on frequency for pristine PC and nanocomposites.

analysis, and the results are shown in Figure 6. All samples are degraded with one weight-loss stage under heating. When ATP-*g*-PMMA is added, thermal decomposition temperature of nanocomposites shifts to a level obviously higher than that of PC, suggesting that thermal stability is enhanced. Meanwhile, a slightly higher decomposition rate of nanocomposites with the increase of particle loading is observed in comparison with that of PC due to the decomposition of the organic component on the surface of ATP-*g*-PMMA. These results may be attributed to the physical barrier effect of ATP in the polymeric network, where ATP impedes the diffusion of micromolecules originating from degradation. On the other hand, ATP bears a native outstanding thermal stability, which can absorb heat through the melting process and retard the thermal degradation of nanocomposites.

Morphology Analysis

FESEM images of fracture surfaces of the PC/ATP-*g*-PMMA nanocomposites are shown in Figure 7. As can be seen from Figure 7(A,B), the morphologies of impact fracture surface vary dramatically when 1 wt % and 5 wt % ATP-*g*-PMMA are added respectively. There is no distinct interface between particles and matrix in nanocomposites containing 1 wt %, which may be attributed to the compatibilization effect of clay in the immiscible PC and PMMA.[38] However, for that containing 5 wt %, hybrid particles are separated from the matrix. It can also be seen from Figure 7(C), a slight aggregation can be observed, and the majority of the ATP-*g*-PMMA particles are rod-like in the diameter range of 80–100 nm consisting of several single rod crystals.

Rheological Properties

The manufacture properties and rheological behavior of nanocomposites were investigated *via* melt-flow index measurement and rheological analysis. Figure 8 presents the results of MFR. As increasing the content of ATP-*g*-PMMA from 0 to 7 wt %, the MFR of nanocomposites increases from 10.24 g/10 min to 13.83 g/10 min, especially the maximum value 15.40 g/10 min at 5 wt %. It is well known that the higher MFR value means the lower viscosity of melt in the course of processing. This phenomenon may correlate with the microstructure of nanocomposites, thus, rotational rheometer was employed to illustrate the effect of ATP-*g*-PMMA on the composites melt.

Figure 9 shows the dependence of complex viscosity on the angular frequency of pristine PC and PC/ATP-*g*-PMMA nanocomposites. Each curve includes two stages, small frequency dependence stage at low frequency and obvious shear thinning stage at high frequency. The viscosity curves for 1 wt % and 3 wt % ATP-*g*-PMMA have similar dependencies as the neat PC, the change of complex viscosity during the first stage is almost ignorable, approximating to the Newtonian fluid; whereas, 5 wt % and 7 wt % ATP-*g*-PMMA present slight shear thinning behavior. This is in accordance with the theoretical and experimental observation for nanofiber and nanoclay reinforced composites.[39–42] In nanocomposites embedded with nanofiller, it is believed that filler–polymer and filler–filler interactions increase with the increase of filler content, which forms the so-called percolation network structure. This structure plays a dominant role in rheological behavior for nanocomposites, resulting in that the Newtonian area of melt is narrowed or even disappeared as a considerable loading of nanofiller. According to the

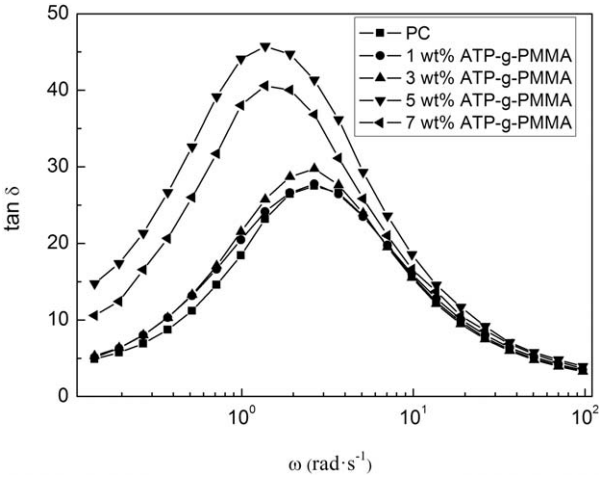

Figure 10. Dependence of tan (δ) on frequency for pristine PC and nanocomposites.

results in FTIR, the chemical interaction between PC and ATP-*g*-PMMA is negligible, only the physical entanglement effect and filler–filler interaction should be taken into consideration here. On the other hand, surface grafting of polymer can alleviate the filler–filler interaction so that to avoid aggregation and decrease the effective volume of ATP-*g*-PMMA. Therefore, the contribution of the above effects to the formation of percolation network structure is limited.

Different from the previous results reported on PC nanocomposites,[43,44] it is interesting to find that the complex viscosity of PC nanocomposites decreases dramatically and then increases as increasing the content of ATP-*g*-PMMA, this phenomenon is similar to the results we have reported.[45,46] In this system, PC macromolecule chains adhered on the surface of nanoparticles are limited, resulting in the faster orientation of rigid nanoparticles under the shear force. Thus, the disentanglement effect caused by the orientation of ATP-*g*-PMMA is more pronounced especially virgulate filler. What's more, the grafting PMMA layer makes interfaces slide more easily. These factors decrease the complex viscosity of nanocomposites.

Figure 10 gives the relationship between the angular frequency and the tan δ for PC and PC/ATP-*g*-PMMA nanocomposites with respect to the oscillatory frequency. The decrease in loss factor is more significant at low frequency, which matches the results of complex viscosity. Nanocomposites exhibit more liquid-like viscoelastic behavior compared with the pristine PC, probably indicating a better mobility of polymer chains.

CONCLUSIONS

The objective of the present study was to examine the effects of hybrid particles ATP-*g*-PMMA on the mechanical properties, thermal stability, rheological behavior of nanocomposites, and the interaction between PC and ATP-*g*-PMMA. In which, PMMA anchoring the surface of ATP was performed *via* RAFT graft polymerization, and ATP-*g*-PMMA was incorporated into PC by melt blending method. The FTIR revealed there was no chemical action between PC and ATP-*g*-PMMA. The thermal stability of nanocomposites was enhanced significantly compared with pristine PC. FESEM micrographs of nanocomposites suggested that the aggregation of ATP-*g*-PMMA and phase separation were sharpened with the increase of particle loadings. For the nanocomposites containing 5 wt % ATP-*g*-PMMA, the disentanglement and interface slip effects increased the mobility of polymer chains, which resulted in the lower complex viscosity and higher loss factor. In conclusion, despite the loss in mechanical properties, rod-like modified particles such as ATP-*g*-PMMA percentage around 1–5 wt % presents a practical advantage to enhance the thermal stability, especially the processability of nanocomposites. On this basis, reducing or even reversing the loss in mechanical properties is the direction for future research.

ACKNOWLEDGMENTS

This work was financially supported by the Project Funded by the Priority Academic Program Development of Jiangsu Higher Education Institutions (PAPD).

REFERENCES

1. Usuki, A.; Hasegawa, N.; Kato, M. *Adv. Polym. Sci.* **2005**, *179*, 135.
2. Sharma, R. K.; Gulati, S.; Pandey, A.; Adholeya, A. *App. Catal. B-Environ.* **2012**, *125*, 247.
3. Kadib, A. E. I.; Bousmina, M. *Chem. Eur. J.* **2012**, *18*, 8264.
4. Bitinis, N.; Hernández, M.; Verdejo, R.; Kenny, J. M.; Lopez-Manchado, M. A. *Adv. Mater.* **2011**, *23*, 5229.
5. Dhibar, S.; Kar, P.; Khatua, B. B. *J. Appl. Polym. Sci.* **2012**, *125*, 601.
6. Legrand, D. G.; Bendler, J. T. Handbook of Polycarbonate Science and Technology; Marcel Dekker: New York, **2000**.
7. Jindal, P.; Pande, S.; Sharma, P.; Mangla, V.; Chaudhury, A.; Patel, D.; Singh, B. P.; Mathur, R. B.; Goyal, M. *Composites: Part B.* **2013**, *45*, 417.
8. Yahyaei, H.; Mohseni, M.; Bastani, S. *J. Sog-gel. Sci. Technol.* **2011**, *59*, 95.
9. Phuong, V. T.; Coltelli, M. B.; Cinelli, P.; Cifelli, M.; Verstichel, S.; Lazzeri, A. *Polymer* **2014**, *55*, 4498.
10. Xia, X. C.; Zhang, Q. P.; Wang, L.; He, S.; Yang, M. B. *Polymer* **2014**, *55*, 6399.
11. Eceiza, A.; Martin, M. D.; Caba, K. D.; Kortaberria, G.; Corcuera, M. A.; Mondragon, I. *Polym. Eng. Sci.* **2008**, *48*, 297.
12. Wu, D. F.; Wu, L. F.; Zhang, M.; Wu, L. *Eur. Polym. J.* **2007**, *43*, 1635.
13. Wang, S. F.; Hu, Y.; Wang, Z. Z.; Yong, T.; Chen, Z. Y.; Fan, W. C. *Polym. Degrad. Stab.* **2003**, *80*, 157.
14. Suin, S.; Shrivastava, N. K.; Maiti, S.; Khatua, B. B. *Eur. Polym. J.* **2013**, *49*, 49.
15. Suin, S.; Maiti, S.; Shrivastava, N. K.; Khatua, B. B. *Mater. Des.* **2014**, *54*, 553.
16. Suin, S. K.; Khatua, B. B. *Ind. Eng. Chem. Res.* **2012**, *51*, 15096.
17. Rama, M. S.; Swaminathan, S. *Ind. Eng. Chem. Res.* **2010**, *49*, 2217.
18. De la orden, M. U.; Pascual, D; Antelo, A.; Arranz-Andrésc, J.; Lorenzo, V.; Urreaga, J. M. *Polym. Degrad. Stab.* **2013**, *98*, 1110.
19. Bradley, W. F. *Am. Miner.* **1940**, *25*, 405.
20. Guan, Y.; Song, C.; Gan, Y. T.; Li, F. M. *Agron. Sustain. Dev.* **2014**, *34*, 657.
21. Guggenheim, S.; Adams, J. M.; Bain, D. C.; Bergaya, F.; Brigatti, M. F.; Drits, V. A.; Formso, M. L. L.; Galan, E.; Kogure, T.; Stanjek, H. *Clay. Miner.* **2006**, *54*, 761.
22. Guerra, D. L.; Silva, E. M.; Airoldi, C. *Process. Saf. Environ.* **2010**, *88*, 53.
23. Tian, H. J.; Guo, Q. J.; Xu, D. Y. *J. Power. Sources.* **2010**, *195*, 2136.
24. Wang, R. G.; Li, Z.; Wang, Y. M.; Liu, W. B.; Deng, L. B.; Jiao, W. C.; Yang, F. *Polym. Compos.* **2013**, *34*, 22.
25. Wang, J. H.; Han, X. J.; Ma, H. R.; Ji, Y. F.; Bi, L. J. *Chem. Eng. J.* **2011**, *173*, 171.

26. Shi, J. S.; Yang, X. J.; Wang, X.; Lu, L. D. *Polym. Test.* **2010**, *29*, 596.
27. Hu, K.; Zheng, K.; Tian, X. Y.; Chen, L.; Sun, L. L.; Shui, X. Y. *J. Macramol. Sci. Part B: Phys.* **2011**, *50*, 846.
28. Gao, X.; Mao, L. X.; Zhang, M. X. *Acta. Mater. Compos. Sinica (China)* **2005**, *22*, 1.
29. Via, M. D.; Morrison, F. A.; King, J. A.; Caspary, J. A.; Mills, O. P.; Bogucki, G. R. *J. App. Polym. Sci.* **2011**, *121*, 1040.
30. Yan, X. L.; Gong, Z. L.; Gong, J.; Gao, S.; Zhang, Z. L.; Wang, B. *Carbon.* **2012**, *50*, 2899.
31. Carroccio, S.; Paglisi, C.; Montaudo, G. *Macromolecules* **2002**, *35*, 4297.
32. Puglisi, C.; Sturiale, L.; Motaudo, G. *Macromolecules* **1999**, *32*, 2194.
33. Yang, H. C.; Pu, H. T.; Gong, F. H. *J. Appl. Polym. Sci.* **2014**, DOI: 10.1002/app.41062.
34. Zhang, L.; Yang, H. C.; Liu, H.; Ni, Q. T.; Gong, F. H. *Polym. Eng. Sci.* **2014**, DOI: 10.1002/pen.23956.
35. Chiefari, J.; Chong, Y. K.; Ercole, F.; Krstina, J.; Jeffery, J.; Le, T. P. T.; Mayadunne, R. T. A.; Meijs, G. F.; Moad, C. L.; Moad, G.; Rizzardo, E.; Thang, S. H. *Macromolecules* **1998**, *31*, 5559.
36. Watts, J. H.; Leadley, S. R.; Castle, J. E.; Blomfield, C. *J. Langmuir* **2000**, *16*, 2292.
37. Percy, M. J.; Michailidou, V.; Armes, S. P.; Perruchot, C.; Watts, J. F.; Greaves, S. J. *Langmuir* **2003**, *19*, 2072.
38. Ray, S. S.; Bousmina, M. *Macromol. Rapid. Comm.* **2005**, *26*, 450.
39. Kitano, T.; Kataoka, T. *Rheol. Acta* **1980**, *19*, 753.
40. Kitano, T.; Kataoka, T.; Nagatsuka, Y. *Rheol. Acta* **1984**, *23*, 20.
41. Zhang, Q.; Lippits, D.; Rastogi, S. *Macromolecules* **2006**, *39*, 658.
42. Solomon, M. J.; Almusallam, A. S.; Seefeldt, K. F.; Somwangthananroj, A.; Varadan, P. *Macromolecules* **2001**, *34*, 1864.
43. Sung, Y. T.; Han, M. S.; Song, K. H.; Jung, J. W.; Lee, H. S.; Kum, C. K.; Joo, J.; Kim, W. N. *Polymer* **2006**, *47*, 4434.
44. Pötschke, P.; Abdel-Goad, M.; Alig, I.; Dudkin, S.; Lellinger, D. *Polymer* **2004**, *45*, 8863.
45. Yang, H. C.; Zhang, L.; Ma, W. Z.; Pu, H. T.; Gong, F. H. *J. Appl. Polym. Sci.* **2014**, DOI: 10.1002/app.41567.
46. Ni, Q. T.; Yang, H. C.; Liu, H.; Ye, Q.; Gong, F. H. *Polym. Mater. Sci. Eng. (China)* **2014**, *30*, 156.